Chemical composition of the graphitic black carbon fraction in riverine and marine sediments at sub-micron scales using carbon X-ray spectromicroscopy.

by

Paul R. Haberstroh[1*], Jay A. Brandes[2], Yves Gélinas[3], Angela F. Dickens[4], Sue Wirick[5], and George Cody[5]

1. Marine Science Institute, The University of Texas at Austin, 750 Channel View Drive, Port Aransas, TX 78373 USA

2. Skidaway Institute of Oceanography, 10 Ocean Science Circle, Savannah, GA, 31411 USA

3. Concordia University, Chemistry and Biochemistry Department, 7141 Sherbrooke St. West, Montreal, Canada H4B 1R6

4. Marine Chemistry and Geochemistry, Woods Hole Oceanographic Institution, Woods Hole, MA 02543 USA

5. Department of Physics, SUNY-Stony Brook, Stony Brook, NY 11794 USA

5. Geophysical Laboratory, Carnegie Institution of Washington, 5251 Broad Branch Road NW, Washington DC 20015 USA

*Author to whom correspondence should be addressed (phaberstroh@mohave.edu)

November 30, 2005

Abstract. The chemical composition of the graphitic black carbon (GBC) fraction of marine organic matter was explored in several marine and freshwater sedimentary environments along the west coast of North America and the Pacific Ocean. Analysis by carbon x-ray absorption near edge structure (C-XANES) spectroscopy and scanning transmission x-ray microscopy (STXM) show the GBC-fraction of Stillaguamish River surface sediments to be dominated by more highly-ordered and impure forms of graphite, together forming about 80% of the GBC, with a smaller percent of an aliphatic carbon component. Eel River Margin surface sediments had very little highly-ordered graphite, and were instead dominated by amorphous carbon and to a lesser extent, impure graphite. However, the GBC of surface sediments from the Washington State Slope and the Mexico Margin were composed almost solely of amorphous carbon. Pre-anthropogenic, highly-oxidized deep-sea sediments from the open Equatorial Pacific Ocean contained over half their GBC in different forms of graphite as well as highly-aliphatic carbon, low aromatic/highly-acidic aliphatic carbon, low aromatic/highly aliphatic carbon, and amorphous forms of carbon. Our results clearly show the impact of graphite and amorphous C phases in the BC fraction in modern riverine sediments and nearby marine shelf deposits. The pre-anthropogenic Equatorial Pacific GBC fraction is remarkable in the existence of highly-ordered graphite.

1. INTRODUCTION

Black carbon (BC) is comprised of a spectrum of heterogeneous, aromatic and carbon-rich compounds, most of which are thought to be the end products of fossil-fuel combustion and biomass burning (Goldberg 1985, Masiello 2004). In marine sediments much of the BC has been attributed to deposition of soot, though fluxes from weathered kerogens and other soil BC sources, have also been implicated (Suman et al. 1997; Dickens et al. 2004 a). BC compounds can also bind pollutants and organic substances in general and therefore many forms of marine organic matter could become associated with BC-rich particles (Gustafsson et al. 1997; Lee et al. 2004).The net ecological effect of BC formation may be to channel carbon and oxygen away from biomass formation and cycling, into a refractory pool which is poorly mineralized by microbial communities. In addition, recent studies have shown that a fraction of BC in sediments may derive from petrogenic (rock) sources, rather than from combustion (Dickens et al. 2004 a,b). The presence of this recycled BC in sediments may have led to significant overestimates of burial of combustion-derived BC in marine sediments, may bias radiocarbon dating of marine sedimentary organic carbon, and may form a closed loop in the carbon cycle (Dickens et al. 2004 a).

All definitions of BC rely upon the extraction technique employed, e.g., they are operationally defined. However, depending upon the method BC may be produced from non-BC compounds altered by the extraction techniques (Schmidt et al. 2000, 2001; Masiello 2004). The Gélinas et al. (2001) method isolates only the most thermally

recalcitrant forms of BC, generally soot and graphite, resulting in an operationally-defined graphitic black carbon fraction (GBC). This method removes types I and II kerogen, coal, charcoal, as well as other non-GBC organic compounds (Gélinas et al. 2001, Dickens 2004 a). Application of the Gélinas method by Dickens et al. (2004a,b) has shown the GBC in pre-industrial horizons of marine sediments of the Washington Coast Slope to be dense, silt-sized (3-63 μm), and dominated by ^{14}C-depleted fractions, the likely product of weathering of fossilized organic carbon from continental rocks. However, in recent sediments from an urban lake, Wakeham et al. (2004) have shown that GBC derives primarily from fossil fuel combustion. Therefore, GBC potentially can be composed of varying fractions of modern components (soot from natural combustion processes), and ancient ones (new soot from the anthropogenic combustion of fossil fuels, old soot from natural paleofires, and petrogenic sources of GBC) which are likely sub-components of kerogen. Little is known about the particle-scale composition of GBC in natural samples. A detailed characterization of the GBC fraction of the BC pool in a variety of sedimentary environments may help further resolve the relative contributions of the modern and ancient sources to these environments.

GBC and other BC components are inherently difficult to chemically analyze and thus it is not surprising that there have been few studies that examined their chemical structure. Microscopic investigations can chemically-analyze very small amounts of material and have indicated spatial heterogeneity of chemical components in sediment particles (Mitchell 2001; Sommer and Franke 2002; Jamin et al. 2003). X-ray microscopic techniques are particularly promising in the investigation of recalcitrant

particles, since they have small resolution limits (Jacobsen and Kirz 1998). Synchrotron-based X-ray fluorescence microscopy (SXRF) for example has been successful in quantifying a variety of trace element (e.g. Si, Mn, Fe, Ni, Zn, Cr) in bacteria, phytoplankton, and autotrophic- and heterotrophic-flagellates (Kemner et al. 2004; Twining et al. 2003, 2004; Twining and Baines 2004). One particularly useful tool has been Scanning Transmission X-ray Microscopy (STXM), which allows for the non-invasive collection of X-ray Absorption Near-Edge Structure (XANES; or NEXAFS for Near-Edge X-ray Absorption Fine Structure). This combination of microscopy and spectroscopy (spectromicroscopy) can map the abundance of different carbon functional groups within a particle with a current resolution limit of less than 50 nm, minimal "signal averaging" problems, and minor sample handling (e.g. no extraction or derivatization). In C-XANES, carbon functional groups are identified by the energy of absorption of x-ray photons by core-shell (C 1s) electrons, in the pre-ionization energy range of 280-300 eV for C 1s electrons. Recent STXM and C-XANES examinations of sediment trap material from the Arabian Sea material demonstrated four distinct phases: protein, an aliphatic-rich phase, a carboxylic-rich phase, and a phase of complex unsaturated and quinone components (Brandes et al. 2004). Very few BC-like particles were observed in these waters by Brandes et al. (2004).

Since GBC may originate both from erosion of ancient rocks and in modern and ancient combustion processes (Dickens et al. 2004a, b) it is critical to examine GBC from a wide array of sedimentary environments in order to better resolve these possible sources and components. In this work we use C-XANES and STXM to examine natural

GBC samples, isolated from riverine and continental shelf sediments located along the western coast of North America, and in the deep Equatorial Pacific. The objective of this study was to understand the degree of chemical heterogeneity in the structure of GBC in these sedimentary environments to explore whether these techniques may be useful for identifying sources and fates of BC. Most of the GBC samples examined in this work were isolated from surface sediments and are considered to be recent and post-industrial. However, the Equatorial Pacific sediment was determined to be below the sediment mixed-layer depth by ^{210}Pb-dating, and to be pre-industrial by low levels of nuclides from nuclear fallout (Carpenter et al. 1987), by background concentrations of combustion-derived polycyclic aromatic hydrocarbons (Prahl and Carpenter 1984), and by ^{14}C-determined sedimentation rates (Dickens et al. 2004a). The data are used to constrain the chemical composition of GBC and to estimate the relative proportions of carbon in different composition classes from each environments.

2. MATERIALS AND METHODS

2.1 Graphitic Black Carbon Treatment of Sediment Samples

Archived sediment samples were analyzed from a variety of sedimentary end-member environments, which ranged from continental margin sentiments overlain by oxic and suboxic waters, a river sediment from a small watershed, a margin sediment from a different small river system, and a highly-oxidized deep-sea sediment (Fig. 1; Table 1). Surface sediments were collected from the Stillaguamish River (Dickens et al.

2004 a,b) and the Eel River Margin (Blair et al. 2004). The Washington Coast Slope samples were from 0-6 cm sediment depth, while Mexico Margin samples were collected from 0-5 cm sediment depth (Dickens et al. in press). The Equatorial Pacific 9^{o}N sample was from 9-10 cm sediment depth (Hammond et al 1996). The total organic carbon (TOC) and GBC fractions were isolated from whole sediments by the method of Gélinas et al. (2001). As described below, due to time constraints of C-XANES analysis from 8 to 12 C-XANES particle images were examined in each sediment environment (Table 1).

For GBC isolation the sediments were demineralized by sequential treatments with 1 N HCl, and between two to eight treatments with 1 N HCl/10% HF in order to expose organic matter trapped within mineral matrices to further chemical treatment. Hydrolysable organic carbon was then removed by treatment with O_2-free trifluoroacetic acid and HCl to reduce the possibility that condensation products would form during the thermal oxidation step (Maillard 1913). The remaining material was subjected to thermal oxidation at 375^{o}C for 24 h. The method selectively isolates highly-condensed BC (primarily soot) and graphite while destroying charcoal, coal and type I and II kerogen. The weight % of TOC and GBC fractions were determined directly with a Carlo-Erba elemental analyzer. Gélinas et al. (2001) conservatively estimate the standard deviations in GBC concentrations to be ± 15%.

2.2 Sediment Sample Sectioning for C-XANES

Small (~100 μg) subsamples of the GBC fraction were embedded in reagent grade elemental sulfur by briefly heating (~120^{o}C) a mixture of fine S^{o} grains and sample on a clean glass slide until the mixture melted into a drop. Upon cooling the drop was removed from the slide with a razor, and fixed to an epoxy mount using cyanoacrylate glue. The drop was then sectioned into 130 nm (± 5 nm) thick slices using a Leica Ultra-CutTM ultramicrotome and a diamond knife, and the slices were then transferred to silica monoxide-supported TEM grids for storage and analysis (Flynn et al. 2003; Brandes et al. 2004).

2.3 STXM and C-XANES Analyses

Images and stacks were collected using the scanning transmission x-ray microscope located on beamline X1-A1 (outboard branch) at the National Synchrotron Light Source, Brookhaven National Laboratory (Winn et al. 2000). Complete details on the design, operation and capabilities of the microscope are described in Feser et al. (2000, 2001). Briefly, synchrotron-generated monochromatic x-ray radiation is focused by a Fresnel zone plate onto a sample with a beam diameter of 45 nm. The sample stage is moved in the xy-plane using a piezo stage so that an x-ray transmission absorption map of the sample is scanned and recorded. The microtomed sections of the material surviving the GBC method represent a large sub-set of the total particles surviving the GBC method, and within each section all carbon-containing particles were examined by C-

XANES. Initially two to twenty images of similar size and at a fixed energy (usually 290 eV) were collected to locate regions of interest (ROI) containing significant absorption in the microtome section. The collective area of all of the ROI for a particular sample section covered the entire particle area. These ROI were subsequently mapped in xy-energy space by sequential collection of several hundred images (collectively called a "stack"), usually spanning from 280 eV to 320 eV (Jacobsen et al. 2000). Occasional unplanned termination of the x-ray beam necessitated truncation of our stack collection to 280-300 eV. The number of these particle image stacks for each sediment environment ranged from 8 to 12 (Table 1).

Typically images were collected at the following energy levels: every 0.2 eV from 280 eV to 284 eV; followed by 0.1 eV from 284 eV to 292 eV, followed by 0.33 eV steps to 300 eV (Jacobsen et al. 2000). When instrument time allowed, additional images were collected at 0.5 to 1.0 eV steps between 300 and 320 eV. The wider spacing in eV steps beyond 300 eV was done to save time, since C-XANES typically do not show an fine features in these regions. These numerous images were aligned, using an automated image alignment program which optimized the location of each image relative to the others using features of strong contrast (Jacobsen et al. 2000).

Pixel sizes ranged from 50 x 50 nm, to 200 x 200 nm, depending on the sample. The dwell times were usually kept to 1 to 3 ms per pixel, depending upon the x-ray flux at a particular energy, and to provide as low a radiation dosage to samples prior to entering the XANES region where detailed spectral information is critical to identifying

the chemistry of each sample (Brandes et al., in review). Typical stack analysis times ranged from approximately 2 to 6 h. Principle component analysis (PCA) was used to orthogonalize and noise-filter the spectromicroscopy data (Lerotic et al. 2004). Cluster analysis was then used to classify pixels according to spectral similarity, and to extract representative, cluster-averaged spectra with good signal-to-noise ratios, and to obtain gradations of the concentration of these spectra at each pixel (Lerotic et al. 2004). In this manner C-XANES spectra and maps of regions of similar composition can be extracted from the data.

Comprehensive C-XANES studies of polymers and other well-characterized compounds have permitted robust criteria for peak absorption energy assignments (Ade and Urquhart 2002; Dhez et al. 2003). Peak energy assignments for common carbon functional groups are listed in Table 2. For carbon K-shell electrons, the near-edge absorption bands extend from 280 to 295 eV, and correspond to transitions to both unoccupied π^* (antibonding) and low lying σ^* orbitals. The peak width is generally given by the lifetime of the photoexcited transition, with transitions at lower energies relative to the ionization edge having longer lifetimes. In general, the lowest energy absorption bands, from around 284-285 eV, are for functional groups with unusually low energy π^* states, e.g. quinones. An aromatic or unsaturated C atom bonded to another C atom has a strong 1s-$1\pi^*$ transition at about 285 eV. As more electron-drawing elements are added (e.g., pyridinic nitrogen) or substituted to unsaturated C (e.g., carbonyl or oxygen), the binding energy of the 1s electron is increased. This binding energy increase shifts the 1s-$1\pi^*$ transitions of aromatic C to higher energies, up to about 286 eV for carbonyl and

nitrogen, and up to 286.9 eV for oxygen (e.g., as in phenols). For carboxyl functional groups bonded to saturated C the two oxygens result in a shift of the 1s-1π^* transition up to 288.5 eV. For carboxyamide the 1s-1π^* transition is a bit lower, at 288.2 eV. Saturated carbon has broad absorption band around 287.5-288 eV due to the σ^* transition, ethers and alcohols exhibit a π^* transition at 289.5 eV.

The cluster optical density spectra generated by PCA for a particle can be used to estimate the amount of carbon characterized by that spectra (M. Lerotic and C. Jacobsen., personal communication). It should be noted that the following method calculates the relative, and not absolute, amounts of C within clusters analyzed on the same instrument. As X-rays travel through a sample they are absorbed as a function of the Lambert-Beer law, as given by

$$I(E) = I_0(E)e^{-\mu(E)t}$$

where I(E) is the transmitted flux at energy E, I_0 is the incident flux, - μ(E) is the linear absorption coefficient at an energy E, and t is the sample thickness. To calculate carbon mass per unit area two energies must be selected from the cluster optical density spectrum: one from below the absorption edge (E_1) and one from above the absorption edge (E_2), and both energies need to be far from the pre- and post-edge XANES features, respectively. Mass per unit area can then be given as

$$m = \rho\,[(E_2/E_1)^3 \ln\{I(E_2)/I_0(E_2)\} - \ln\{I(E_1)/I_0(E_1)\}] / [\mu_{henke}(E_1) - (E_2/E_1)^3 \mu_{henke}(E_2)]$$

where ρ is the mass density of the desired component (e.g. carbon) and μ_{henke} is the mass absorption coefficient (Henke et al. 1993, Gullikson 2001). The total mass M can be calculated from the mass per unit area m, the number of pixels N_{pixels}, and the pixel size A_{pixel} as

$$M = m \cdot N_{pixels} \cdot A_{pixel}$$

Ideally I_2 would be in the 320-340 eV region, above most of the σ^* resonances. However time and instrument constraints often precluded the collection of data above 300 eV. Therefore total carbon was estimated for each cluster spectral type by subtracting the optical density at 280 eV from the average of the optical density from 295-300 eV. Although absorptions at 295-300 eV are considerably higher than post-edge values at 320-340 eV, this difference is consistent across a variety of chemical compositions. C-XANES spectra was examined from a library of 11 polymeric compounds (www.physics.ncsu.edu/stxm/polymerspectro). The average absorption at 295-300 eV was 20% ± 10% higher than at the highest eV scanned, 320 eV. In addition 15 of the 58 spectra examined were collected up to 320 eV, and the average percent difference between the absorption at 295-300 eV compared to that at 320 eV fell in the range noted above. Therefore the absorption density-difference between the average at 295-300 eV and that at 280 eV, was multiplied times the areal fraction of that cluster of the total particle image size, and this product multiplied times the pixel size (μm^2). This allowed a comparison of the relative amount of carbon in different compositional categories (see

Results) in each sedimentary environment. Since most of the variables between the samples were internally-normalized, the degree of uncertainty in this technique is dependent on the variability of the calculation in mean absorbance from 295 to 300 eV, which was approximately ± 1-3% of the mean absorbance values.

3. RESULTS

The sedimentary environments sampled had a wide range of TOC and GBC weight percent of total sediment mass (Table 1). TOC weight percent was lowest for the Stillaguamish River (0.14%), and highest for the Mexico Margin (7.19%), while the GBC weight percent was lowest for the pre-anthropogenic Equatorial Pacific sediment (0.012%), and highest in the Eel River Margin (0.20%). The percent GBC of TOC was highest in the Stillaguamish River sediment (31.0%), lower in the Eel River Margin (17.6%), and very low in the Mexico Margin (0.20%). The Washington Coast Slope and Mexico Margin had about equal percent GBC of TOC (about 3.4 to 3.8%).

For purposes of comparison we present the cluster spectra for some well-characterized substances: graphite (Figure 2.A.), NIST standard reference 2975 diesel soot (Figure 2.B., C.), and melanoidin produced by the reaction of lysine and glucose (Figure 2.D.). Graphite cluster spectra characteristically have a sharp peak for unsaturated carbon-carbon bonds near 285 eV and a sharp σ^* exciton absorption peak near 291.6 eV. The exciton is a bound excited state with a long lifetime compared to the atomic de-excitation mechanisms, and so the excitonic peaks are very narrow (Ma et al. 1993; see

Table 2). The graphite spectra also exhibit a well-defined asymmetric absorption peak at 292.8 eV, reflecting the transition to the many superimposed σ^* states. The diesel soot shows the presence of both aromatic and aliphatic carbon groups, i.e. at 287.6-288.2 eV for the 1s-3p/σ^* transition for C-H, and 289.5 eV for the 1s-3p/σ^* transition for C-OH (Figure 2B., C.) while melanoidin (Figure 2.D.) has significant spectral content in the aromatic carbon region (285 eV), aromatic alcohol (about 286.5 eV), and carboxyl region (288.6 eV). In diesel soot the lack of a sharp σ^* exciton absorption peak near 291.6 eV, and the absence of the characteristic σ^* absorption peak at about 292.8 eV, is indicative of the lack of significant spatial extent of graphene aromatic rings (see Table 2 and Discussion).

The C-XANES spectra of observed GBC classes from the sedimentary environments examined are presented in Figure 3. The cluster spectra were divided into six specific classes, I-VI, based upon similarity to the cluster spectra of reference compounds and those presented in Gago et al. (2000, 2001) and Jiménez et al. (2003). Binning of particle classes within stack clusters was chosen based on criteria given in Figure 3. For example, a region was considered highly ordered graphite if it contained well defined peaks at 295, 291.6 and 292 eV, with few or no spectral features between 286 and 290 eV. Impure graphitic carbon exhibited strong and defined 285 and 292 eV features together with strong absorption features in the 287-290 eV region. Amorphous carbon consistently had strong but poorly separated absorption features in the 285-290 eV region, followed by a broad increase in the 293-296 eV range (much broader than the graphite transition in this region). This material was quite distinct from impure graphite

in that impure graphite had a clear separation in absorbance peaks between 285 and 287 eV, while amorphous C did not (Figure 3). Occasionally non-graphitic, non-amorphous carbon types were observed that corresponded more closely to types observed in marine organic matter (Brandes et al. 2004). All of these forms were characterized by a much higher 287:285 ratio than either graphitic or amorphous carbon, indicating a higher proportion of aliphatic and/or carboxylic acid C. Spectral distinctions between classes were obvious and in no case did we observe a compound class that did not clearly fall into one of these six classes.

All the particles in each of the microtomed thin-sections from the homogeneously-mixed subsample of the material surviving the GBC-method were examined to ensure a representative sampling of the whole sample. For each of the five sedimentary environments, we examined between 8 and 12 image stacks (Table 1). This relatively limited number of observations was necessitated by the long amount of time required for each analysis (3-6 h per observation), so our examinations represent a large sub-set of the total sample particles surviving the GBC-method. Most of the image stacks also included more than one distinct particle. In addition, the stack images from some of the sedimentary environments were more particle-rich than in others. The total particle area examined varied from approximately 1300 μm^2 for the deep Equatorial Pacific 9oN to 7800 μm^2 for Washington Coast Slope sediments. The chemical mapping of GBC components did not exhibit a "ring" or "crust" of more oxidized material on the surfaces of the particles. The lack of observable surface alteration compared to particle interiors in

our chemical maps is a strong indication that the GBC treatment method of Gélinas et al. (2001) affects the entire particle.

Within each sedimentary environment the relative amounts of carbon in each of the six spectral cluster classes was calculated (see Methods and Table 3). GBC in the Stillaguamish River sediment is dominated by highly-ordered and impure forms of graphitic C, collectively constituting over 80% of the total C, with the remainder primarily in the form of more aliphatic carbon (17%). In contrast, the GBC-fraction in the sediments of the Eel River Margin is dominated by amorphous C (72%) with lesser amounts of impure graphitic C (27%). The GBC-fraction in the sediments from the Washington Coast Slope and in the Mexico Margin entirely consist of amorphous C (97-100%). In the Equatorial Pacific 9^{o}N sediments the GBC-fraction has a much broader distribution of the spectral classes, containing impure graphitic C (35%) and highly-organized graphitic C (21%), but also appreciable amounts of highly aliphatic C, low aromatic, highly aliphatic C (12%) and low aromatic, highly acidic aliphatic C (8%) and amorphous C (8%; Table 3). These percent differences exceed the variability introduced by the C mass determination method, which was approximately ± 1-3%. We have also confirmed the presence of aliphatic C in the Stillaguamish River sediment GBC by FTIR (Gélinas, unpublished data).

We also estimated the presence of inorganic material in the samples based on their characteristic C-XANES cluster spectra, which have a constant absorbance (with intensity related to sample thickness) in the C-XANES region, from 280 to 300 eV

(Brandes et al. 2004). We are currently restricted to estimating their abundance to the percent area of the C-XANES image. Very little inorganic material was detected in the GBC-fraction of sediments from the Eel River Margin. In rare cases distinct particles of inorganic material were observed in the GBC-fraction from the Stillaguamish River and Mexico Margin sediments. However, the paucity of inorganic material demonstrated that the demineralization procedures used by Gélinas et al. (2001) were effective. Further resolution of inorganic components and absolute estimation of C was further complicated by the existence of unsublimated S^o, used during the sample preparation stage, which is indistinguishable at the C-edge from relict mineral phases. Thus no direct estimates of inorganic content were made for this investigation.

4. DISCUSSION

Continental shelves and slopes contain approximately 90% of the OC buried in the oceans, and the processes which control this burial influence Earth's atmospheric chemistry and global climate over geological time scales (Berner, 1982; 1989; Hedges and Keil 1995). Active margins in particular have steep landscapes and are often drained by short mountainous rivers that facilitate the rapid delivery and burial of terrestrial OC to the continental shelf and slope (Blair et al. 2003, 2004). The Eel River Margin, and to a lesser extent the Washington Coast Slope, can be considered to be river-dominated sedimentary systems as they receive considerable sediment influx from the Eel River and Columbia River watersheds, respectively. The Columbia River has a much larger and longer watershed than the Eel River, but both impact their respective margins as

important sites of terrestrial OC burial (Berner 1982; Hedges and Keil 1995; Goñi et al. 2005). Enhanced sedimentation rates, high fluxes of terrigenous nutrients, elevated inputs of mineral surfaces and land-derived recalcitrant organic matter all combine to help sequester carbon in these regions. The organic matter in river-dominated margins has been shown to be highly heterogeneous in composition with allochthonous OC including freshwater algae, vascular plant debris, soil organic matter, ancient kerogen and fossilized carbon from sedimentary rocks, and autochthonous OC consisting of marine phytoplankton debris, zooplankton fecal material, and marine bacteria (Masiello and Druffel 2001, 2003, Blair and Aller 2004).

Our analyses of sedimentary GBC illuminate the high degree of chemical heterogeneity of the GBC fraction in the different sedimentary environments and suggest possible linkages to terrestrial sources. However, the admittedly limited number of samples analyzed by C-XANES and STXM do not permit robust conclusions on the sources or fates of the GBC fraction of BC. In the Eel River watershed kerogen, exposed in the uplifted Mesozoic-Tertiary Franciscan Complex, is rapidly eroded, transported, and buried on the margin (Blair et al. 2003, 2004). Of the marine sediments analyzed in the present work the Eel River Margin had the highest weight percent of GBC (0.205%) and percent GBC of TOC (17.6%), and almost 30% of this GBC was graphite (Table 3). These findings suggest that this GBC derives primarily from rock OC and are consistent with this site being heavily impacted by deposition of sub-soil materials eroded away from the Eel River watershed (Blair et al. 2003). Similarly, we found that a very large portion of TOC in the Stillaguamish River sediment was GBC (31%) and most of this

GBC was highly-ordered graphite (45%). The Stillaguamish River is another small, mountainous river and is fed by glaciers, and the dominance of graphite in the TOC of this sediment clearly indicates that much or most of the OC in this sediment derives from sedimentary rock OC. The lowest GBC weight percent values (0.012-0.016%) were found in the Mexico Margin and Equatorial Pacific sediments, both areas which experience very low input of terrestrial OC (Dickens et al. 2004 a). The composition of GBC in these two environments is remarkably different however, since Mexico Margin GBC is almost all amorphous C, while Equatorial Pacific 9-10 cm GBC is comprised of a wide variety of GBC classes (Table 3). Similarly, the GBC of the Washington Coast Slope and the Eel River Margin are both dominated by amorphous carbon (Table 3).

The Equatorial Pacific Ocean site ($8^{o}55$'N, $139^{o}52$' W) is a highly oxidized, open-ocean site that is remote from the typical processes which create highly-ordered graphite. The East Pacific Rise hydrothermal vent field has been identified however as the source of crystalline graphite found approximately 300 m from the ridge axis (Jedwab and Boulègue 1984) but the metaliferrous sediments typical of this and other vent fields were not detected at the Equatorial Pacific 9^{o}N sampling location. Therefore the presence of graphitic forms of GBC in the pre-anthropogenic sediments of the deep Equatorial Pacific, far from any significant fluvial or hydrothermal vent input, supports an aeolian mode of GBC transport, possibly via dust mobilized by desert storms. Aeolian inputs of terrestrial organic carbon, while difficult to determine, appear to have delivery rates to the sediments comparable to those from marine-derived processes, and have been shown to be geochemically significant (Zafiriou et al. 1985; Peltzer and Gagosian 1989;

Eglinton et al. 2002). The most likely source of the highly-ordered graphite in the open Equatorial Pacific Ocean may be continental dust, possibly from central Mexico, and transported by the NE trade winds and storms to the open Pacific Ocean.

It is possible that the other non-amorphous, non-graphitic forms of organic carbon found in the Equatorial Pacific GBC may be artifacts from the GBC method, formed by the condensation of recent marine biomacromolecules, and which could dilute the age of the GBC material to a relatively young ^{14}C-determined age of about 10,000 years, rather than 40,000 years for nearshore sediments (Dickens et al. 2000a). Gustaffson et al. (2001) has shown the production of BC values from thermal oxidation of diatom exudates, and whereas the Gélinas et al. (2001) method effectively removes most non-BC forms of carbon, it is possible that it may produce small amounts of BC for samples that are relatively low in pyrogenic carbon or fossil graphitic carbon (Simpson and Hatcher 2004). Some of the aliphatic cluster spectra types (e.g. types I, II, and III) were somewhat similar to the melanoidin produced through a reaction between lysine and glucose (i.e., Figure 2, and Brandes et al. 2004), but much more detailed examination of different melanoidin reaction types should be conducted. This research is also underway.

What processes and/or sources of GBC are shared between the Mexico Margin, the Washington Coast Slope and the Eel River Margin surface sediments, that results in predominantly amorphous C in the GBC fraction? Given the much higher burial rates usually found on continental shelves as compared to deep-sea environments, it is tempting to speculate that amorphous GBC forms, and not graphitic forms, may dominate

GBC burial in the ocean. However, more work is needed to delineate the possible source mechanisms leading to the transport and burial of amorphous GBC. It is, however, important to note that this form of GBC has not been previously observed and was not predicted to survive the GBC extraction treatment.

Based on the very old ^{14}C-based age of the GBC (11,000-41,000 years old) in riverine- and coastal marine-sediments, as well as a heavy ^{13}C value, Dickens et al (2004 a) concluded that the GBC source for Washington Coast Margin must be fossilized graphite weathered from continental rocks, carried to the oceans and re-deposited to marine sediments. Our analyses were constrained mostly to modern sediments, yet are partially consistent with Dickens et al. (2004 a) conclusions, as we clearly show that the GBC-fraction in the sediments of the one mountainous river we sampled to be predominantly highly-ordered graphitic carbon. Yet our analyses show the GBC from the Washington Coast Margin was not crystalline graphite but amorphous carbon. Since GBC is well-known to be recalcitrant, then what could be the source and chemical structure of the amorphous carbon form of GBC, which leads to its persistence in such widely different sedimentary environments? We consider three hypothetical sources of the amorphous carbon:1) petrogenic graphite which is transformed to amorphous carbon during its transport to marine sediments, 2) soot from combustion of either fossil fuels or biomass, and 3) a form of non-graphitic kerogen, which has not undergone the extensive metamorphic processes necessary to form the highly-ordered graphene planes characteristic of petrogenic graphite.

Petrogenic graphite formation commonly occurs as a result of organic matter conversion under natural heating during low-grade metamorphism, or metamorphism of carbonate-rich rocks or organic-rich sediments, or via precipitation from natural carbon-bearing fluids such as those containing CO_2, CO, and/or CH_4 (Frost et al. 1989; Person et al. 1996; Luque et al. 1998; Duba et al. 2001, Jödicke et al. 2004; Pucéat et al. 2004). Studies by Gago et al. (2000, 2001) used highly oriented pyrolytic graphite as precursor material and produced amorphous carbon by ion beam assisted decomposition. This amorphous carbon was examined by C-XANES and produced spectra identical to some of our spectra. Amorphous carbon has been distinguished from highly-ordered graphite as a progressive decrease of the π* exciton (at 285.4 eV), with the appearance of several π* states of similar intensity due to the increase in the sp^2-related π* states in the region between 285 to 288 eV (Gago et al. 2000, 2001). The decrease in the π* exciton is apparently due to the reduction of graphite domain size in the amorphisation process, as theoretical modeling of the XANES spectra found a dependence of the exciton intensity with plane-cluster size (Ahuja et al. 1996). The decrease of the π* intensity as the ordered graphite becomes progressively amorphous was likely due to the increase of sp^3 hybridized sites at the expense of the sp^2 hybridized sites. Possible mechanisms consistent with the increase in the sp^3/sp^2 ratios with amorphisation could include 1) formation of vacancies in the graphitic basal planes, by removal of certain carbon atoms and leaving dangling carbon bonds; 2) formation of five- and seven-member rings that curve the basal planes and connect dangling bonds; and 3) promotion of sp^3 sites that can also distort the flat basal plane geometry and can cross-link different planes (Gago et al. 2001; Jiménez et al. 2003).

Is it possible that the complete dissociation of the graphitic basal planes into amorphous carbon is a dominant process controlling the GBC found in the continental margin samples? Ion beam assisted deposition is not a direct analogue for any natural process. Perhaps photo-oxidation has the ability to leave the graphitic structure intact enough to resist oxidation by the GBC isolation method, but disrupted enough to appear amorphous via the C-XANES analysis. The presence of impure- and highly-ordered graphite in the Eel River GBC suggests that the putative graphite oxidative-dissociation mechanism may not had enough time to act before being rapidly buried, because of the intense erosion and burial of OC in this watershed. In contrast the longer residence time of carbon in the Columbia River system before deposition on the North American margin may promote extensive amorphisation.

Another possible source of the pre-anthropogenic GBC in the Equatorial Pacific 9-10 cm sediment might be soot from the combustion of C_4 grasses (Eglinton et al. 2002, Dickens et al 2004 a). At the most extreme end of the combustion product spectrum, highly graphitized soot spheroids are formed from extensive recombination of small free radicals of acetylenic and aromatic molecules within the flame (Goldberg 1985). The soot spheroids possess onion-like layers and layers of graphite formed by sp^2 hybridized carbon, but curved due to the presence of sp^3 hybridized carbon (Dobbins et al. 1998; Schmidt and Noack 2000). Less intensive combustion of vegetative biomass may produce more randomly-oriented stacks of a few graphitic layers (Heidenreich et al. 1968). Soot particle nanostructure, which includes the graphene layer plane dimensions, their

tortuosity, and relative orientation, can dictate its reactivity towards oxidation (Vander Wal and Tomasek 2003). At the edge of the short (< a few nm) stacks of graphene plate-segments (termed "crystallites") the potential carbon sites (aryl C-H bonds) are well known to be most susceptible to oxidation compared to the carbon atoms within the basal plane, which have only shared π electrons forming chemical bonds (Palmer and Cullis 1965; Vander Wal and Tomasek 2003). The degree of curvature of the crystallites also increases the susceptibility of the carbon atoms to oxidation, exposing weakened C-C bonds, as bond strain increases as the orbitals overlap and the electronic stabilization is decreased (Dresselhaus et al. 1996). The soot particles should be quickly oxidized by ozone and other atmospheric oxidants, creating hydrophilic carboxylic acids and aromatic polyacids on their exterior surfaces, and thus promoting soot particle solubilization (Chughtai et al. 1991; Decesari et al. 2002). At present we have only limited C-XANES and STXM examinations of soot, and those were derived from diesel combustion (Figure 2 B. and C). We did not observe these type of spectra in Equatorial Pacific (nor any other location) sediments. However, it is possible that soot derived from vegetation fires may have a less condensed structure and thus have a different C-XANES spectrum. While soot may have small domains of graphene layers and crystallites their small dimensions will not lead to the large absorbance we observed for unsaturated carbon at 291.8 eV, which is more characteristic of multiple layers of aromatic rings typical of petrogenic graphite. Furthermore, soot does not exhibit the strong absorption between 285.5 and 287 eV that we observe in our amorphous C class, and thus cannot be the unaltered sources of this material. Soot can partially survive the GBC-fractionation method yet NMR examinations of soot treated by the Gélinas method revealed a loss of aliphatic

components and a preservation of aromatic components (Gélinas, personal communication), suggesting that the amorphous phase is not derived from chemically-altered soot. Further work at the N- and O- edges by XANES on GBC should distinguish whether its origin is petrogenic graphite, which should contain very little N, or fossil fuel combustion products, which should contain significant N and O components.

We can not reject the possibility that the GBC found along the coastal margins is neither transformed petrogenic graphite nor combustion products, but is instead a non-graphitic form of kerogen. Kerogen is an inherently-complex macromolecular mixture (Tissot and Welte 1978; Hedges 1992) that may include petrogenic graphite and many molecularly-uncharacterizable compounds. While kerogen of types I and II does not survive the GBC-treatment method (Dickens et al. 2004a,b), a fraction of type III kerogen, which comprises a large aromatic component (Tissot and Welte, 1984) might be thermally-resistant and could contribute to the GBC isolate. This could consist of a sort of proto-graphite that is condensed enough to survive the GBC method but irregular enough to appear as graphite by C-XANES.

Clearly a more detailed understanding of GBC sources, transport and diagenesis should include at the least a more systematic and thorough sampling of the rivers of the both coasts of the North American continent proper and their related margins. Combustion products of grasses and woods also need a more thorough examination by C-XANES and STXM. This type of research is underway and will be presented in a later work

5. CONCLUSIONS

Our results show a clear impact of graphite and amorphous C phases in the BC fraction in modern riverine sediments and nearby marine shelf deposits, and also in the pre-anthropogenic sediments in the open ocean. This is consistent with the findings of Dickens et al. (2004a,b), that sedimentary GBC may not involve a significant contribution by combustion products. Sedimentary environments along continental margins have a GBC fraction of BC which is characterized by more disordered graphite and amorphous carbon. The Equatorial Pacific GBC fraction is remarkable in the existence of highly-ordered graphite, but they also appear to contain significant aliphatic components. C-XANES and PCA are clearly powerful analytical tools in the delineation of the composition of GBC

Acknowledgements. This work was supported by NSF grants OCE-0221295 and OCE-0118036 (JAB), and OCE-9310364 (SGW), by a NSF Graduate Research Fellowship to A.F.D., and the Canadian National Science and Engineering Research Council to Y.G. The National Synchrotron Light Source is a Department of Energy supported facility. The authors wish to thank Chris Jacobsen, Mirna Lerotic and Holger Fleckenstein (SUNY) for their patient assistance in the operation of the STXM, and in PCA and cluster analysis, and Marie Helene Veilleux (CU) for FTIR analyses. This work is dedicated to the memory of John I. Hedges, mentor and friend.

REFERENCES

Ade H. and Urquhart, S.G. (2002) NEXAFS spectroscopy and microscopy of natural and synthetic polymers. In: *Chemical Applications of Synchrotron Radiation* (ed. T.K. Sham), Advanced Series in Physical Chemistry, Vol. **12**, World Scientific Publishing, Singapore.

Ahuja R., Brühwiler P.A., Wills J.M., Johansson B., Mårtensson N., and Eriksson O. (1996) Theoretical and experimental study of the graphite 1s x-ray absorption edge. *Phys. Rev. B* **54**(**20**), 14396-14404.

Berner R.A. (1982) Burial of organic carbon and pyrite sulfur in the modern ocean: its geochemical and environmental significance. *American Journal of Science* **282**, 451-473.

Berner R.A. (1989) New model for atmospheric oxygen over Phanerozoic time. *Am. J. Sci.* **289**, 333-361.

Blair N.E., Leithold E.I., Ford S., Peeler K., Holmes J., and Perkey D. (2003) The persistence of memory: the fate of ancient sedimentary organic carbon in a modern sedimentary system. *Geochim. Cosmochim. Acta* **63**, 63-73.

Blair N.E., Leithold E.I., and Aller R.C. (2004) From bedrock to burial: the evolution of particulate organic carbon across coupled watershed-continental margin systems. *Marine Chemistry* **92**, 141-156.

Brandes J.A., Lee C., Wakeham S., Peterson M., Jacobsen C., Wirick S., and Cody C. (2004) Examining marine particulate organic matter at sub-micron scales using scanning transmission X-ray microscopy and carbon X-ray absorption near-edge structure spectroscopy. *Marine Chemistry* **92**, 107-121.

Carpenter R., Beasely T.M., Zahnle D., and Somayajulu B.L.K. (1987) Cycling of fallout (Pu, ^{241}Am, ^{137}Cs) and natural (U, Th, ^{210}Pb) radionuclides in Washington continental slope sediments. *Geochim et Cosmochim. Acta* **51**, 1897-1921.

Chughtai A.R., Jassmin J.A., Peterson J.H., Stedman D.H., and Smith D.M. (1991) Spectroscopic and solubility characteristics of oxidized soots. *Aerosol Science and Technology* **15**, 112-126.

Cody, G.D., Botto, R.E., Ade, H. and Wirick, S. (1996) The application of soft x-ray microscopy to the in-situ analysis of sporinite in coal. *International Journal of Coal Geology* **32**, 69-86.

Cody, G.D., Ade, H., Wirick, S., Mitchell, G.D. and Davis, A. (1998) Determination of chemical-structural changes in vitrinite accompanying luminescence alteration using C-NEXAFS analysis. *Organic Geochemistry* **28**, 441-455.

Decessari S., Facchini M.C., Matta E., Mircea M., Fuzzi S., Chughtai A.R., and Smith D.M. (2002) Water soluble compounds formed by oxidation of soot. *Atmospheric Environment* **36**, 1827-1832.

Dhez O., Ade H., and Urquhart S.G. (2003) Calibrated NEXAFS spectra of some common polymers. *Journal of Electron Spectroscopy and Related Phenomenon* **128**, 85-96.

Dickens A.F., Gélinas Y., Masiello C.A., Wakeham S, and Hedges J.I. (2004a) Reburial of fossil organic carbon in marine sediments. *Nature* **427**, 336-339.

Dickens A.F., Gélinas Y., and Hedges J.I. (2004b) Physical separation of combustion and rock sources of graphitic black carbon in sediments. *Marine Chemistry* **92**, 215-223.

Dickens A.F., Baldock J.A., Smernik R.J., Wakeham S.G., Arnarson T.S., Gélinas Y. and Hedges J.I. (in press) Solid-state ^{13}C NMR analysis of size and density fractions of marine sediments: Insight into organic carbon sources and preservation mechanisms. *Geochim. Cosmochim. Acta.*

Dobbins R.A., Fletcher R.A., and Chang H.-C. (1998) The evolution of soot precursor particles in a diffusion flame. Combust. Flame **115**, 285-298.

Dresselhaus M.S., Dresselhaus G., and Eklund P.C. (1996) Science of Fullerenes and Carbon Nanotubes. Academic Press.

Duba A., Mathez E.A., and Shankland T.J. (2001) Workshop addresesses crustal carbon and its effect on electrical conductivity. *EOS, Transactions of the American Geophysical Union* **82**, 456.

Eglinton, T. I., Eglinton, G., Dupont, L., Sholkovitz, E R., Montluçon, D. and Reddy, C. M. (2002) Composition, age, and provenance of organic matter in NW African dust over the Atlantic Ocean. *Geochem., Geophys., Geosyst*., **3**: 1-27.

Feser M., Beetz T., Carlucci-Dayton M. and Jacobsen C. (2000) Instrumentation advances and detector development with the Stony Brook scanning transmission x-ray microscope. In: *X-ray Microscopy: Proceedings of the Sixth International Conference* (eds. W. Meyer-Ilse, A. Warwick and D.T. Attwood), pp. 367-372. American Institute of Physics, Melville, NY.

Feser M., Beetz T., Carlucci-Dayton M. and Jacobsen C. (2001) Scanning transmission soft x-ray microscopy at beamline X-1A at the NSLS - advances in

instrumentation and selected applications. In: *Soft X-ray and EUV Imaging Systems II.* (eds. D.A. Tichenor and J.A. Folta), pp. 146-153. Society of Photo-Optical Instrumentation Engineers, Bellingham, WA.

Flynn G.J., Keller L.P., Feser M., Wirick S., and Jacobsen C. (2003) The origin of organic matter in the solar system: evidence from the interplanetary dust particles. *Geochim. Cosmochim. Acta* **67**(**24**), 4791-4806.

Francis, J.T., and Hitchcock, A.P. (1992) Inner-shell spectroscopy of para-benzoquinone, hydroquinone, and phenol-distinguishing quinoid and benzenoid structures. *Journal of Physical Chemistry* **96**(**16**), 6598-6610.

Frost B.R., Fyfe W.S., Tazaki K., and Chan T. (1989) Grain boundary graphite in rocks and implications for high electrical conductivity in the lower crust. *Nature* **340**, 134-136.

Gago R., Jiménez I., Albella J.M., Climent-Font A., Cáceres D., Vergara V., Banks J.C., Doyle B.L, and Terminello L.J. (2000) Bonding and hardness in nonhydrogenated carbon films with moderate sp3 content. *Journal of Applied Physics* **87**(**11**), 8174-8180.

Gago R., Jiménez I., and Albella J.M. (2001) Detecting with X-ray absorption spectroscopy the modifications of the bonding structure of graphitic carbon by

amorphisation, hydrogenation and nitrogenation. *Surface Science* **482/485**, 530-536.

Gélinas Y., Prentice K.M., Baldock J.A., and Hedges J.I. (2001) An improved thermal oxidation method for the quantification of soot/graphitic black carbon in sediments and soils. *Environ. Sci. Technol.* **35**(**7**), 3519-3525.

Goldberg E.D. (1985) *Black Carbon in the Environment*. John Wiley & Sons, New York, 198 pp.

Goñi M.A., Yunker M.B., Macdonald R.W., and Eglinton T.I. (2005) The supply and preservation of ancient and modern components of organic carbon in the Canadian Beaufort Shelf of the Arctic Ocean. *Marine Chemistry* **93**, 53-73.

Gullikson E. (2001) Mass absorption coefficients. In: *X-ray data booklet* (eds. Thompson A.C. and Vaughn, D.) Center for X-ray optics advanced light source, Lawrence Berkeley National Laboratory.

Gustafsson Ö., Haghseta F., Chan C., MacFarlane J. and Gschwend P.M. (1997) Quantification of the dilute sedimentary soot phase: implications for PAH speciation and bioavailability. *Environ. Sci. Technology* **31**, 203-209.

Gustafsson Ö., Bucheli T.D., Kukulska Z., Andersson M., Largeau C., Rouzand J-N., Reddy C.M., Eglinton T.I. (2001) Evaluation of a protocol for the quantification of black carbon in sediments. *Global Biogeochem. Cycles* **15**, 881-890.

Hammond D.E., McManus J., Berelson W.M., Kilgore T.E., and Pope R.H. (1996) Early diagenesis of organic material in equatorial Pacific sediments: stoichiometry and kinetics. *Deep-Sea Res. II* **43**, 1365-1412.

Hartnett H.H., Keil R.G., Hedges J.I., and Devol A.H. (1998) Influence of oxygen exposure time on organic carbon preservation in continental marine sediments. *Nature* **391**, 572-574.

Hedges J.I. (1992) Global biogeochemical cycles: progress and problems. *Marine Chemistry* **39**, 67-93.

Hedges J.I., and Keil R.G. (1995) Sedimentary organic matter preservation: an assessment and speculative synthesis. *Marine Chemistry* **49**, 81-115.

Heidenreich R.D., Hess W.M., and Ban L.L. (1968) A test object and criteria for high resolution electron microscopy. *J. Appl. Crystallogr.* **1**, 1-19.

Henke B.L, Gullikson E.M., and Davis J.C. (1993) X-ray interactions: photoabsorption, scattering, transmission, and reflection at E = 50-30,000 eV, Z =1-92. *At. Data Nucl. Data Tables* **54**, 181.

Hitchcock, A.P., Horsley, J.A., and Stöhr, J. (1986) Inner shell excitation of thiophene and thiolane-gas, solid, and monolayer states. *Journal of Chemical Physics* **85**(**9**), 4835-4848.

Hitchcock, A.P., and Ishii, I. (1987) Carbon K-shell excitation spectra of linear and branched alkanes. *J. Electron Spectroscopy and Related Phenomena* **42**(**1**), 11-26.

Hitchcock, A.P., and Stöhr, J. (1987) K-shell shape resonances and intramolecular bond lengths-comments on the relationship between shape resonances and bond lengths. *Journal of Chemical Physics* **87**(**5**), 3253-3255.

Hitchcock, A.P., Urquhart, S.G., and Rightor, E.G. (1992) Inner shell spectroscopy of benzaldehyde, terephthalaldehyde, ethyl benzoate, terephthaloyl chloride, and phosgene-models for core excitation of poly(ethylene-terephthalate). *Journal of Physical Chemistry* **96**(**22**), 8736-8750.

Jacobsen C., and Kirz J. (1998) X-ray microscopy with synchrotron radiation. *Nature Structural Biology* **5**, 650-653.

Jacobsen C., Flynn G., Wirick S., and Zimba C. (2000) Soft x-ray spectroscopy from image sequences with sub-100 nm spatial resolution. *Journal of Microscopy* **197**(**2**), 173-184.

Jamin N., Miller L., Moncuit J., Fridman W.H., Dumas P., Teillaud J.L. (2003) Chemical heterogeneity in cell death: combined synchrotron IR and fluorescence microscopy studies of single apoptotic and necrotic cells. *Biopolymers* **72**(**5**), 366-373.

Jedwab, J., and Boulègue, J. (1984) Graphite crystals in hydrothermal vents. *Nature* **310**, 41-43.

Jiménez I., Gago R., and Albella J.M. (2003) Fine structure at the X-ray absorption π^* and π^* bands of amorphous carbon. Diamond and Related Materials **12**, 110-115.

Jödicke H., Kruhl J.H., Ballhaus C., Giese P., and Untiedt J. (2004) Syngenetic, thin graphite-rich horizons in lower crustal rocks from the Serre San Bruno, Calabria (Italy), and implications for the nature of high-conducting deep crustal layers. *Physics of Earth and Planetary Interiors* **141**, 37-58.

Kemner K.M., Kelly S.D., Lai B., Maser J., O'Loughin E.J., Sholto-Douglas D., Cai Z., Schneegurt M.A., Kulpa C.F., and Nealson K.H. (2004) Elemental and redox analysis of single bacterial cells by X-ray microbeam analysis. *Science* **306**, 686.

Kuhlbusch T.A.J., and Crutzen P.J. (1995) Towards a global estimate of black carbon in residues of vegetation firs representing a sink of atmospheric CO_2 and a source of O_2. *Glob. Biogeochem. Cycles* **9**(**4**), 491-501.

Lee C., Wakeham S.G. and Arnosti C., (2004) Particulate organic matter in the sea: The composition conundrum. *Ambio*. **33**(**8**), 565-575.

Lerotic M., Jacobsen C., Schäfer T. and Vogt S. (2004) Cluster analysis of soft x-ray spectromicroscopy data. *Ultramicroscopy* **100**(1-2), 35-57.

Luque F.L., Pasteris J.D., Wopenka B., Rodas M. and Barrenechea J.F. (1998) Natural fluid-deposited graphite: mineralogical characteristics and mechanisms of formation. *American Journal of Science* **298**, 471-498.

Ma Y., Skytt P., Wassadahl N., Glnas P., Mancini D.C., Guo J. and Nordgren J. (1993) Core excitons and vibronic coupling in diamond and graphite. *Phys. Rev. Lett.* **71**(**22**), 3725-3728.

Maillard L.C. (1913) Formation de matières humiques par action de polypeptides sur les sucres. *C.R.-Acad. Sci.* (Paris) **156**, 148-149.

Masiello C.A. and Druffel E. (2001) Carbon isotope geochemistry of the Santa Clara River. *Global Biogeochemical Cycles* **15**, 407-416.

Masiello C.A. and Druffel E. (2003) Organic and black carbon C-13 and C-14 through the Santa Monica Basin sediment oxic-anoxic transition. *Geophysical Research Letters* **30**(**4**) (art.no. 1185).

Masiello C.A. (2004) New directions in black carbon organic geochemistry. *Marine Chemistry* **92**, 201-213.

Mitchell P. (2001) Turning the spotlight on cellular imaging-advances in imaging are enabling researchers to track more accurately the localization of macromolecules in cells. *Nature Biotechnology* **19**(**11**), 1013-1017.

Palmer H.B., and Cullis C.F. (1965) In: *The chemistry and physics of carbon*. (ed. P.L. Walker), **1**, 265, Marcel Dekker, New York.

Peltzer E.T. and Gagosian R.B. (1989) Organic geochemistry of aerosols over the Pacific Ocean. *Chemical Oceanography* **10**, 281-338.

Person A., Bocherens H., Mariotti A., and Renard M. (1996) Diagenetic evolution and experimental heating of bone phosphate. *Palaeogeogr. Palaeoclimatol. Palaeoecol.* **126**, 135-149.

Prahl F.G. and Carpenter R. (1984) Hydrocarbons in Washington coastal sediments. *Estuar. Coast. Shelf Sci.* **18**, 703-720.

Pucéat E., Reynard B., and Lécuyer C. (2004) Can crystallinity be used to determine the degree of chemical alteration of biogenic appetites? *Chemical Geology* **205**, 83-97.

Schmidt M.W.I and Noack A.G. (2000) Black carbon in soils and sediments: analysis, distribution, implications, and current challenges. *Global Biogeochem. Cycles* **14**, 777-793.

Schmidt M.W.I., Skjemstad J.O., Czimczik C.I., Glaser B., Prentice K.M., Gélinas Y., and Kuhlbusch T.A.J. (2001) Comparative analysis of black carbon in soils. *Global Biogeochemical Cycles* **15**(**1**), 163-167.

Simpson M.J. and Hatcher P.G. (2004) Overestimates of black carbon in soils and sediments. *Naturwissenschaften* **91**, 436-440.

Sommer A.P. and Franke R.P. (2002) Near-field optical analysis of living cells in vitro. *Journal of Proteome Research* **1**(**2**), 111-114.

Suman D.O., Kuhlbusch T.A.J., and Lim B. (1997) Marine sediments: a reservoir for black carbon and their use as spatial and temporal records of combustion, Sediment Records of Biomasss Burning and Global Change. *NATO ASI Ser*. 271-293.

Tissot B.P. and Welte D.H. (1978) *Petroleum Formation and Occurrence*. Springer-Verlag, New York.

Twining B.S., Baines S.B., Fisher N.S., Maser J., Vogt S., Jacobsen C., Tovar-Sanchez A., and Sanudo-Wilhelmy S.A. (2003) Quantifying trace elements in individual aquatic protist cells with a synchrotron X- ray fluorescence microprobe. *Anal. Chem.* **75**, 3806-3816.

Twining B.S. and Baines S.B. (2004) Element stoichiometries of individual plankton cells collected during the Southern Ocean Iron Experiment (SOFeX). *Limnol. Oceanogr.* **49**(**6**), 2115-2128.

Twining B.S., Baines S.B., Fisher N.S. and Landry M.R. (2004) Cellular iron contents of plankton during the Southern Ocean Iron Experiment (SOFeX) *Deep-Sea Res.* **51**, 1827-1850.

Urquhart, S.G. and Ade, H. (2002) Trends in the carbonyl core (C 1s, O 1s) $\rightarrow \pi^*$ C=O transition in the near-edge X-ray absorption fine structure spectra of organic molecules. *Journal of Physical Chemistry B* **106**(**34**), 8531-8538.

Vander Wal R.L. and Tomasek A.J. (2003) Soot oxidation: dependence upon initial nanostructure. *Combustion and Flame* **134**, 1-9.

Wakeham, S.G., Forrest J., Masiello C.A., Gélinas Y., Alexander C.R., and Leavitt P. (2004) Hydrocarbons in Lake Washington sediments-a 25 year retrospective in an urban lake. *Environ. Sci. Technol*. **38**(**2**), 431-439.

Winn B., Ade H., Buckley C., Feser M., Howells M., Hulbert S., Jacobsen C., Kaznacheyev K., Kirz J., Osanna A., Maser J., McNulty I., Miao J., Oversluizen T., Spector S., Sullivan B., Wang Y., Wirick S., and Zhang H. (2000) Illumination for coherent soft X-ray applications: the new X1A beamline at the NSLS. *J. Synchrotron Radiation* **7**, 395-404.

Zafiriou O.C., Gagosian R.B., Peltzer E.T. and Alford J.B. (1985) Air-to-sea fluxes of lipids at Enewetak Atoll. *Journal of Geophysical Research* **90**(**D1**), 2409-2423.

Table 1. Sedimentary environments analyzed by STXM and C-XANES.

Description	Location	Water Depth (m)	Sediment Depth (cm)	Number of Particle Images Examined	Total Particle Area Examined (μm^2)	Fraction	Wt. (%)	Percent GBC of TOC (%)
Stillaguamish River, Washington	48°14'N, 121°47' W	1	Surface[1]	9	2768	TOC GBC	0.142 0.044	31.0
Eel River Margin, California Coast	41°02'N, 124°20'W	150	Surface[2]	10	2770	TOC GBC	1.164 0.205	17.6
Washington Coast Slope	46°49'N, 125°W	640	0-6[3]	12	7789	TOC GBC	2.70 0.0929	3.4
Mexico Margin (Suboxic Zone)	22°41.8'N, 106°28.6'W	395	Surface[3]	12	5506	TOC GBC	7.19 0.016	0.2
Equatorial Pacific 9°N	8°55'N, 139°52' W	5000	9-10[4]	8	1305	TOC GBC	0.31 0.0118	3.8

[1]Location described in Dickens et al. (2004 a,b). [2]Described in Blair et al. (2004). [3]Described in Dickens et al. (in press). [4]Location described in Hammond et al. (1996).

Table 2. Approximate energy ranges for the primary absorption peaks at the carbon 1s edge.

Band	Peak Energy (eV)	Transition	C-Functional Group Assignment
1	283.0-284.5	1s-1π^*	Benzo quinone
2	285.0	1s-1π^*	Unsaturated/Aromatic or olefin C=C
3	285.5-286.5	1s-1π^*	Aromatic C=O or Pyridinic C
4	286.5-287.3	1s-1π^*	Aromatic C-OH
5	287.4-288.0	1s-1π^*	Ketone Carbonyl R-(C=O)-R’
6	287.6-288.2	1s-3p/σ^*	Aliphatic C-H
7	288.3	1s-1π^*	Amide –(NH_2)-C=O
8	288.4-288.7	1s-1π^*	COOR
9	289.5	1s-3p/σ^*	Aliphatic C-OH
10	290.0	1s-2π^*	Aromatic COOR
11	290.45	1s-4p/σ^*	Aliphatic C-H
12	292.8	1s-σ^*	C-C, aromatic
13	296.5	1s-σ^*	C-C, aliphatic

Sources: Francis and Hitchcock (1992), Hitchcock et al. (1986, 1992), Hitchcock and Ishii (1987), Hitchcock and Stöhr (1987), Cody et al. (1996, 1998), Urquhart and Ade (2002), George Cody (pers. commun. 2004).

Table 3. Distribution of six categories of carbon in GBC method-treated marine and riverine sediments, based on cluster spectra.

Carbon Type	Stillaguamish River (%)	Eel River Margin (%)	Washington Coast Slope (%)	Mexico Margin (%)	Equatorial Pacific 9 °N (%)
I. Highly Aliphatic	16.8	0	0	0	17.0
II. Low Aromatic, Highly Acidic, Aliphatic	1.1	0	0.3	2.7	7.7
III. Low Aromatic, Highly Aliphatic	2.3	0	0	0	11.8
IV. Amorphous	0	71.5	99.7	97.3	7.8
V. Impure Graphitic	34.8	26.9	0	0	35.1
VI. Highly Organized Graphitic	44.9	1.6	0	0	20.6

FIGURES

Figure 1. Map of sampling sites (denoted by star symbols): A. Stillaguamish River, Washington, B. Eel River Margin, C. Washington Coast Slope, D. Mexico Margin, and E. Equatorial Pacific 9 ^{o}N.

Figure 2. Cluster spectra of separate particles for A. graphite, B.,C. two particles of NIST standard reference 2975 diesel soot particles, and D. melanoidin produced by the reaction of lysine and glucose (originally presented in Brandes et al. 2004).

Figure 3. Cluster spectra classes of GBC method-treated sediment particles.

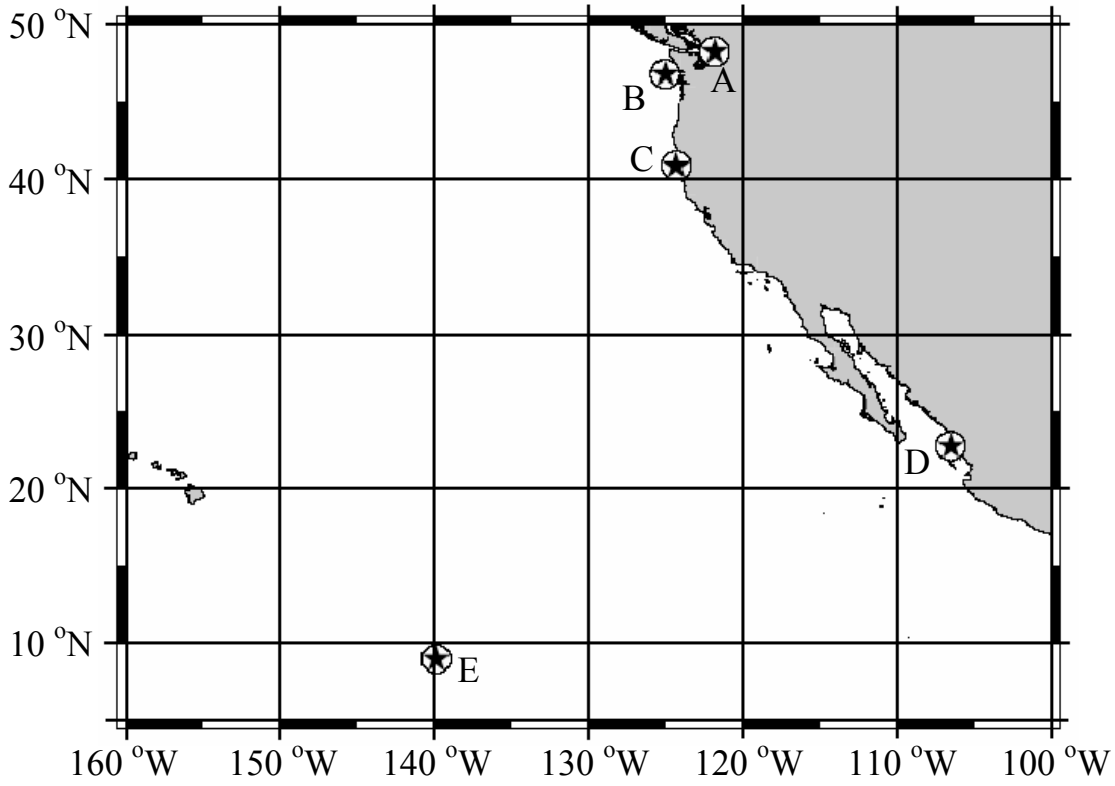

Figure 1. Map of sampling sites (denoted by star symbols): A. Stillaguamish River, Washington, B. Eel River Margin, C. Washington Coast Slope, D. Mexico Margin, and E. Equatorial Pacific 9 °N.

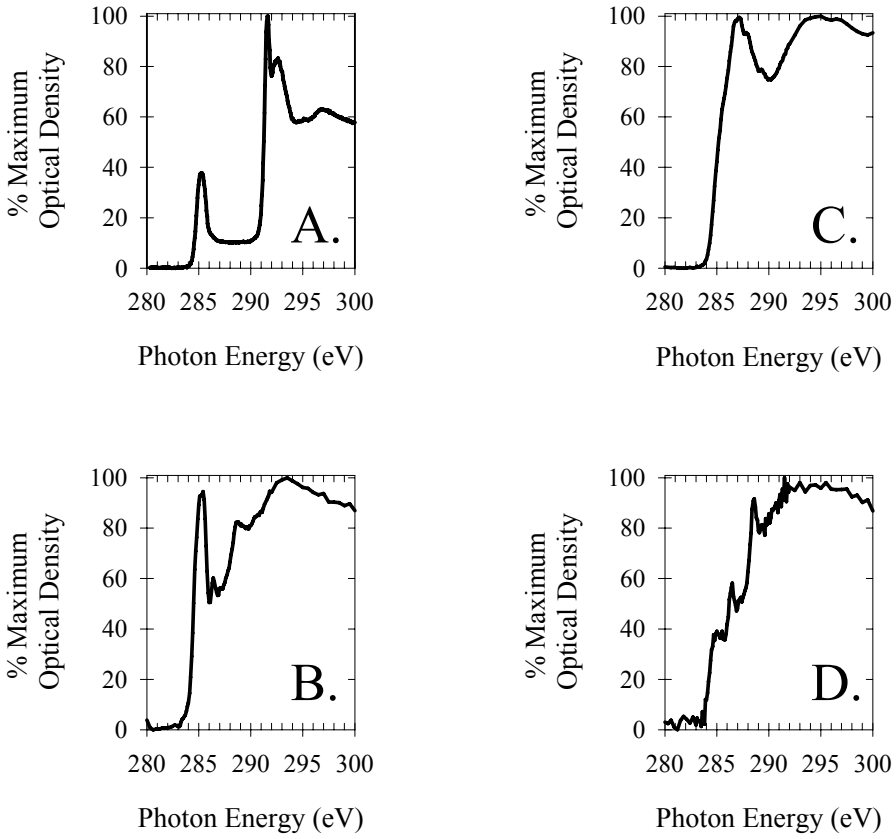

Figure 2. Cluster spectra of separate particles for A. graphite, B.,C. two particles of NIST standard reference 2975 diesel soot particles, and D. melanoidin produced by the reaction of lysine and glucose (originally presented in Brandes et al. 2004).

Class I. Highly aliphatic carbon (little or no absorption peak at 285 eV; large post-287 eV absorption shoulder).

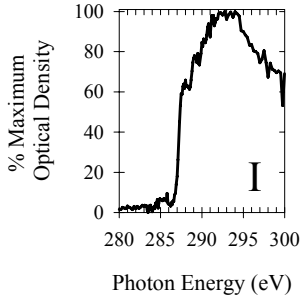

Class II. Low aromatic, acidic, alippatic carbon (similar to Class I but with a small but significant peak at 285 eV, and a very sharp narrow peak at 288.6 eV).

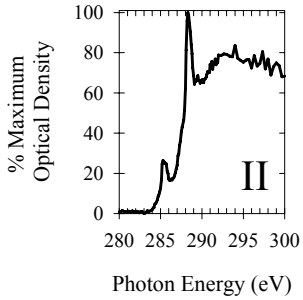

Class III. Low aromatic, highly aliphatic carbon (similar to class I but with a significant peak at 285 eV, and no peak at 288.6 eV).

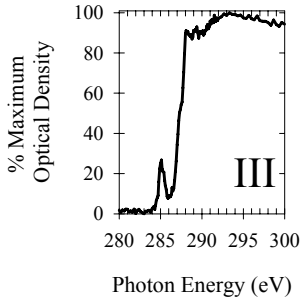

Class IV. Amorphous carbon (large broad adsorption shoulder at 285 eV, little or no decrease in intensity at 286 eV, followed by high absorption from 285-290 eV, and a gradual rise in absorption to the 293 eV region).

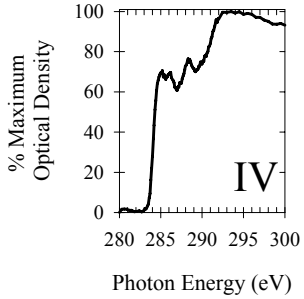

Class V. Impure graphite carbon (three well separated peaks at 285, 288, and 292 eV, with a sharp increase in absorption between 291 and 292 eV, and a small or non-existent 291 eV exciton peak).

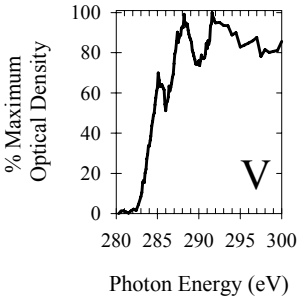

Class VI. Highly-ordered graphite carbon (prominent peak at 285 eV, sharp exciton peak at 291.6 eV, and well-defined peak at 292 eV).

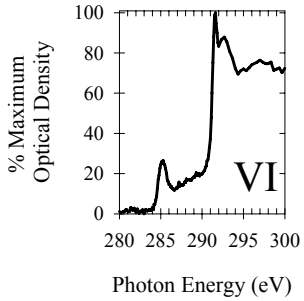

Figure 3. Cluster spectra classes of GBC method-treated sediment particles.